Reduction of the (001) Surface of γ-V_2O_5 Compared to α-V_2O_5

M. Veronica Ganduglia-Pirovano* and Joachim Sauer

Institut für Chemie, Arbeitsgruppe Quantenchemie, Humboldt Universität zu Berlin, Unter den Linden 6, D-10099 Berlin, Germany

Received: August 20, 2004; In Final Form: October 15, 2004

The defect-free γ-V_2O_5(001) surface and ordered structures of oxygen vacancies have been studied for a wide range of defect concentrations, Θ ($^1/_6$ monolayer (ML) $\leq \Theta \leq$ 1 ML), combining density functional theory and statistical thermodynamics. The γ polymorph of V_2O_5 is characterized by two structurally different vanadium sites, V_A and V_B. The V_A sites having a weaker bond to an adjacent crystal layer are easier to reduce. Up to $^1/_2$ ML, the V_A defect structures with defects aligned along the [010] direction are increasingly more stable as in α-V_2O_5(001). At higher defect concentrations, the different coordination of the V_B vanadium atoms at the γ-V_2O_5 surface causes an increase in the vacancy formation energy of ~0.8 eV/atom at $\Theta = 1.0$ compared to $\Theta = {}^1/_2$. For α-V_2O_5, this increase amounts to 0.2 eV/atom only. Under conditions (low oxygen partial pressures and high temperatures) at which the α-V_2O_5(001) surface would be fully reduced, the γ-V_2O_5-(001) surface is only partially reduced. The presence of surface vanadyl oxygen groups at V_B sites may change the surface reactivity compared to that of α-V_2O_5(001).

I. Introduction

α-V_2O_5 is a widely used industrial catalyst for a variety of chemical reactions such as the oxidation of hydrocarbons and sulfur dioxide.[1,2] The oxidation involves Mars−van Krevelen[3] redox cycles using lattice oxygen as reactive intermediates. This conclusion is supported by isotopic labeling studies and by transient-response experiments.[4,5] Mechanistic studies have shown that reduced V centers (V^{III} or V^{IV}) are present at low concentrations during steady-state catalysis.[5,6] The number of reduced centers, that is, the extent of reduction of vanadium oxides during catalytic oxidation, correlates with the turnover frequency, as recently demonstrated for the specific case of oxidative dehydrogenation of propane.[7,8] Thus, reducibility is related to the performance of the catalysts, and this renders an investigation of oxygen removal from well-characterized vanadia surfaces of particular interest.

Recently, we have examined the formation of oxygen vacancies at the (001) surface of α-V_2O_5, which is accompanied by the creation of reduced V centers, by density functional theory (DFT).[9] Further, we assessed the stability of reduced surfaces in thermodynamic equilibrium with an O_2 environment at finite temperatures. We found that, under reducing conditions starting from isolated defect sites up to $^1/_2$ monolayer (ML), the formation of vacancy structures with a favored alignment along the [010] direction is preferred. The vacancy formation energy for concentrations higher than $^1/_2$ ML up to 1.0 ML increases by 0.2 eV/atom only. This suggests that the initial reduction of half of the vanadyl sites may lead to a concerted reduction of the whole surface. The facile reduction of the α-V_2O_5(001) surface is due to substantial vacancy induced structure relaxations leading to the formation of V−O−V bonds between the layers of the α-V_2O_5 crystal.

In the present work, reduction of the V_2O_5(001) surface is investigated by DFT for the polymorph γ. γ-V_2O_5 was first prepared by Cocciantelli et al.[10] by chemical deintercalation of lithium from a γ-LiV_2O_5 bronze. As α-V_2O_5, γ-V_2O_5 has a layered structure of VO_5 pyramids but with two inequivalent vanadium sites. Its electronic structure has been recently investigated using electron energy-loss spectroscopy and DFT calculations.[11] A recent synthesis of V_2O_5 nanorods and nanowires by the reverse micelle technique[12,13] yielded the γ-V_2O_5 phase. Hence, γ-V_2O_5 is a prototype for well-defined nanosized model catalysts and understanding the influence of the crystallographic distortions in γ-V_2O_5 compared to α-V_2O_5 will contribute to understanding differences in their function as oxidation catalysts. In this paper, we will show that the extent of reduction of the γ-V_2O_5(001) surface differs significantly from that of the closely related α-V_2O_5(001) surface under reducing conditions, namely, $T \gtrsim 800$ K and ultrahigh vacuum (UHV).

II. Computational Details and Models

Calculations are based on spin-density functional theory (DFT)[14,15] and employ a plane-wave basis set as implemented in the Vienna ab initio simulation package (VASP)[16−19] up to a 800 eV cutoff. Exchange and correlation are treated with the PW91 generalized-gradient approximation.[20] The electron−core interaction is described by the projector augmented wave (PAW) method as proposed by Blöchl.[21] Core radii of 0.6 and 0.8 Å are used for the oxygen s and p states, respectively. For vanadium, a core radius of 1.2 Å is used and the 3p states are treated as valence states.

The γ-V_2O_5(001) surface is modeled using the supercell approach. We adopt a two-layer (001)-oriented slab with a vacuum region of ~10 Å. Oxygen vacancies are studied for defect concentrations of $\Theta = {}^1/_6$, $^1/_4$, $^1/_3$, $^1/_2$, $^3/_4$, and 1.0 ML with a (1 × 3), (1 × 2), and (1 × 1) surface periodicity. In total, 15 structures have been investigated. The vacancies are created by removing surface oxygen atoms from one side of the slab.

The Brillouin-zone (BZ) sampling is based on the Monkhorst−Pack scheme.[22] A (2 × 6 × 1) grid has been used for the

* To whom correspondence should be addressed. E-mail: vgp@chemie.hu-berlin.de.

10.1021/jp046233k CCC: $30.25
Published on Web 12/08/2004

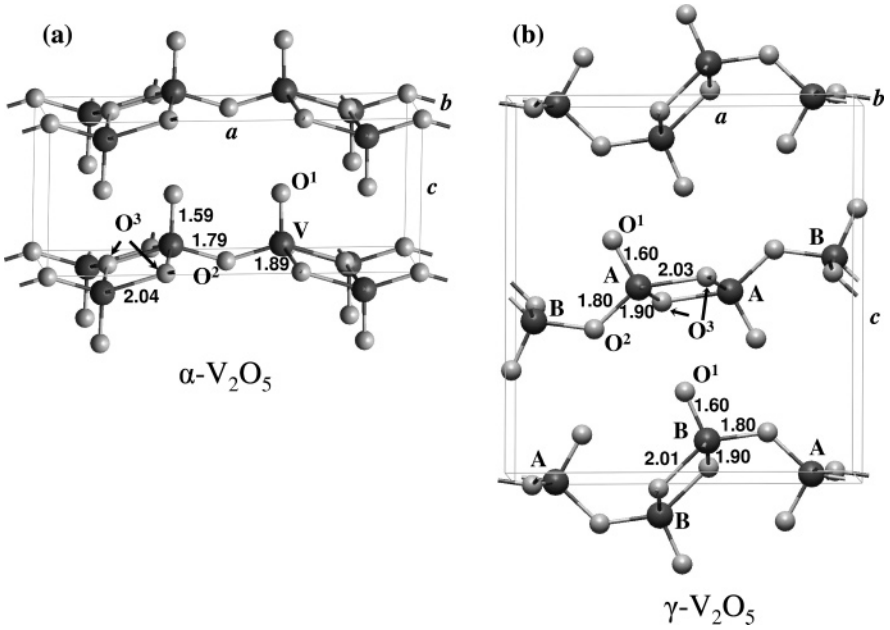

Figure 1. (a) α-V_2O_5 and (b) γ-V_2O_5 crystal structures. *a*, *b*, and *c* of the orthorombic unit cells are parallel to the [100], [010], and [001] directions, respectively. V and O atoms are depicted as dark and light gray circles, respectively. O^1, O^2, and O^3 denote the single, 2-fold, and 3-fold coordinated oxygen atoms, respectively. A and B indicate the two inequivalent vanadium sites in γ-V_2O_5. The bond lengths are in angstroms.

(1 × 1) primitive surface unit cell. These are 12 *k*-points that do not include the $\bar{\Gamma}$-point. For the (1 × 3) and (1 × 2) surface unit cells, grids have been chosen so as to obtain the same sampling of the reciprocal space ((2 × 2 × 1) and (2 × 3 × 1) meshes, respectively) and thus to maintain the same accuracy when comparing the vacancy formation energies at different defect concentrations. The relaxation of the ionic positions into the ground state is performed within a quasi-Newton scheme. All atoms are allowed to relax. The accuracy of calculations of oxygen vacancy formation energies with these parameters (slab thickness, *k*-point grid, and cutoff) was already tested in ref 9 for the closely related α-V_2O_5 case and is therefore not discussed here in any further detail. Selected calculations for reduced γ-V_2O_5(001) surfaces using a thicker slab (three layers), a denser *k*-point grid, and a higher cutoff indicated that the calculations are as well-converged as those of ref 9 for α-V_2O_5.

The total energies of the isolated O_2 molecule, which is involved in the calculation of the average vacancy formation energy (see eq 1), have been calculated in a tetragonal cell of side lengths $a = 10$ Å, $b = 11$ Å, and $c = 12$ Å with Γ-point sampling of the Brillouin zone (other parameters as described above). The binding energy per O atom in O_2 is 3.13 eV/atom[23] and the bond distance 1.234 Å. The experimental results are 2.59 eV/atom (obtained after adding the contributions due to zero-point vibrations to the $T = 0$ K value) and 1.207 Å, respectively.[24] The overestimation of the binding energy and the bond distance is in agreement with earlier density functional calculations that used gradient-corrected functionals.[25,26]

III. Structure of γ-V_2O_5 and Its (001) Surface

The γ polymorph of V_2O_5 forms a layer-type orthorhombic lattice. The unit cell contains 28 atoms (4 formula units). As in α-V_2O_5, double chains of VO_5 pyramids parallel to the *b*-axis exist (see Figure 1). Within a layer in α-V_2O_5, the vanadyl (apical) oxygen atoms of the double chains are oriented along the *c*-axis, forming up- and down-oriented pairs, whereas they alternate up and down individually in the γ-V_2O_5 phase. Additionally, the pyramids are tilted against each other so that the vanadyl bonds are no longer oriented along the *c*-axis. As a consequence, two structurally inequivalent V sites exist, V_A and V_B. Both are coordinated to one vanadyl oxygen, O^1, one bridging oxygen atom, O^2, and three 3-fold coordinated oxygen atoms, O^3. The V_A sites have an additional weak coordination to the vanadyl oxygen of a V_B site in an adjacent layer, as in α-V_2O_5. In contrast, at V_B sites, the VO_5 pyramids are oriented in such a way that no weak interaction with a vanadyl oxygen atom in an adjacent layer exists.

TABLE 1: Calculated and Experimental Lattice Parameters (in Å) of Bulk γ-V_2O_5 Compared with Those for Bulk α-V_2O_5

bulk γ-V_2O_5	*a*	*b*	*c*
this work	10.274	3.592	11.180
exptl[a]	9.946	3.585	10.042
bulk α-V_2O_5	***a***	***b***	***c***
calcd[b]	11.550	3.576	4.836
exptl[c]	11.512	3.564	4.368

[a] Reference 10. [b] Reference 9. [c] Reference 28.

Cell-shape minimizations that included the simultaneous optimization of the fractional coordinates have been performed for several fixed volumes, and the equilibrium volume has been obtained by fitting to the Murnaghan equation of state.[27] After an additional minimization of the cell shape and fractional coordinates at the calculated equilibrium volume, the values $a = 10.274$ Å, $b = 3.592$ Å, and $c = 11.180$ Å have been obtained. For this calculation, a (2 × 6 × 2) *k*-mesh has been used. In Table 1, these values are compared with the experimental values[10] and with corresponding values for bulk α-V_2O_5 (refs 9 and 28 for the calculated and experimental values, respectively). Our calculated energy difference between bulk α-V_2O_5 and γ-V_2O_5 is 0.06 eV/formula unit.[29] The calculated energies of formation, $E_f^{V_2O_5} = [E_{V_2O_5}^{bulk} - 2E_V^{bulk} - {}^5/_2E_{O_2}]$, are −13.36 eV/formula unit (this work) and −16.41 eV/formula unit (ref 9) for polymorphs γ and α, respectively. $E_{V_2O_5}^{bulk}$, E_V^{bulk}, and E_{O_2} are the total energies of the γ- and α-V_2O_5 bulk phases, metallic body-centered cubic (bcc) vanadium, and the O_2 molecule, respectively. The experimental heat of formation of α-V_2O_5 at 298 K is −16.07 eV/formula unit.[30] Similar differ-

TABLE 2: Calculated V−O Bond Distances at the Different Vanadium Sites (in Å) for the Bulk γ-V_2O_5 Structure Compared with the Experimental Values[a]

bond	bulk γ-V_2O_5 exptl[b]	bulk γ-V_2O_5 this work	γ-V_2O_5(001) this work
V_A-O^1	1.547	1.598	1.598
V_A-O^2	1.726	1.800	1.796
V_A-O^3	1.891	1.896	1.898
$V_A-O^{3'}$	1.986	2.034	2.029
$V_A-O^{1'}$	2.714	3.401	3.422
V_B-O^1	1.581	1.598	1.591
V_B-O^2	1.847	1.799	1.810
V_B-O^3	1.896	1.902	1.904
$V_B-O^{3'}$	1.972	2.010	2.013

[a] $V_A-O^{1'}$ corresponds to the weak bond between V_A sites and the vanadyl oxygen of the adjacent layer. The calculated V−O bond distances at the γ-V_2O_5(001) surface correspond to the local surroundings of the VO_5 pyramids sticking out of the surface. [b] Reference 10.

ences between the energies of formation of two bulk phases, namely, α-Al_2O_3 and κ-Al_2O_3, have been calculated using the same density functional (PW91) (0.09 eV/formula unit (ref 31) and 0.08 eV/formula unit (ref 32)). The measured enthalpy difference is 0.16 eV/formula unit (ref 33).

The PW91 calculated lattice parameters *a*, *b*, and *c* deviate from the experimentally observed values by approximately 3, 1, and 11%, respectively. For α-V_2O_5, these deviations are 2, 1, and 11%, respectively.[9] The interaction between the crystal layers in both γ-V_2O_5 and α-V_2O_5 is of the van der Waals type, resulting in a flat potential energy surface. Present DFT methods do not properly account for these weak (dispersion) interactions,[34,35] and this explains the larger deviations in the calculated *c*-lattice parameter. Similar results have been obtained for the interlayer binding in MoS_2[36] and in graphite.[37]

The computed V−O bond distances are virtually identical for V_A and V_B sites (see Figure 1 and Table 2) and agree well with the corresponding computed distances in α-V_2O_5 ($V-O^1 = 1.60$ Å, $V-O^2 = 1.79$ Å, $V-O^3 = 1.89$, and $V-O^{3'} = 2.04$ Å (ref 9)). However, the experimental $V-O^1$ and $V-O^2$ distances show larger differences between V_A and V_B sites, 0.03 and 0.12 Å, respectively. Only the average of a given bond distance for V_A and V_B sites is close to the corresponding experimental distance in α-V_2O_5 ($V-O^1 = 1.58$ Å, $V-O^2 = 1.78$ Å, $V-O^3 = 1.88$, and $V-O^{3'} = 2.02$ Å (ref 28)).

The above-mentioned weak interactions between the layers result in small relaxations upon cleavage of the bulk structure to create the (001)-oriented surface. The outermost V_B-O^1 distances shorten by <0.01 Å, the V_B-O^2 distances become larger by approximately the same amount, and among the $V-O^3$ distances changes are even smaller (see Table 2). Moreover, the calculated surface energies of 0.025 and 0.040 J/m^2 (ref 9) for the relaxed (001) surfaces of γ-V_2O_5 and α-V_2O_5, respectively, and the corresponding values 0.030 and 0.048 J/m^2 for the bulk-truncated surface geometries correlate with the weak nature of the interlayer bonding. The (001) plane is the easy cleavage plane for both γ-V_2O_5 and α-V_2O_5. Indeed, atomically clean α-V_2O_5(001) surfaces can be easily obtained by either pushing a razor blade into the crystal[38] or pulling off very thin layers using Scotch tape.[39]

IV. Reduced γ-V_2O_5(001) Surfaces

The formation of vanadyl oxygen vacancies on the γ-V_2O_5-(001) surface was investigated at six different concentrations, $\Theta = 1/6, 1/4, 1/3, 1/2, 3/4$, and 1.0 ML. Figure 2 shows the considered structures.

The average vacancy formation energy as a function of vacancy concentration, $\Theta = N_{vac}/N_{tot}$, is given by

$$E_f^{(1/2)O_2}(\Theta) = \frac{1}{N_{vac}}\left[E_{vac}(\Theta) - E_{clean} + N_{vac}\frac{1}{2}E_{O_2}\right] \quad (1)$$

where N_{vac} and N_{tot} are the actual and maximum number of vacancies in the surface unit cell and $E_{vac}(\Theta)$, E_{clean}, and E_{O_2} represent the total energies of the reduced surface slab, the defect-free surface slab, and the free oxygen molecule, respectively. A positive value of $E_f^{(1/2)O_2}$ indicates that the vacancy formation is endothermic.

Table 3 summarizes the calculated average O vacancy formation energies at the γ-V_2O_5(001) surface, before and after vacancy induced relaxations are considered. Figure 3 compares the lowest values of $E_f^{(1/2)O_2}$ at each concentration on γ-V_2O_5-(001) to those for the α-V_2O_5 surface[9] after relaxation (lower part). The symbols at the top of Figure 3 show the corresponding values if the geometry is kept fixed at the defect-free surface positions. For these unrelaxed structures, the dependence of the O vacancy formation energy on the vacancy concentration is weak, as for α-V_2O_5(001).[9] If we reduce either V_A or V_B sites at the γ-V_2O_5 surface up to 1/2 ML, the values of $E_f^{(1/2)O_2}$ are by ~0.15 eV/atom lower for V_B sites (see Table 3). This is presumably due to the fact that the vanadyl oxygen atom at V_B sites lies further out of the surface. The corresponding values for α-V_2O_5(001) lie approximately in the middle of that ~0.15 eV/atom energy interval.[9] However, after relaxation, due to the presence of V_B sites at the γ-V_2O_5(001) surface, we find a stronger dependence of the vacancy formation energy on the defect concentration than on the α-V_2O_5 surface.

For isolated sites ($\Theta = 1/6$ ML), the relaxation effect is ~0.3 eV/atom at a V_B site, while at a V_A site the effect is ~6 times larger (see Table 3). Such large relaxation effects have been found for isolated vanadyl defect sites at the α-V_2O_5 surface and attributed to the formation of a bond between the α-V_2O_5 crystal layers at the defect site.[9] Figure 4b shows the formation of an interlayer bond for V_A sites at the γ-V_2O_5 surface that results from the inversion of the VO_5 pyramid at the defect site. The resulting V−O bond lengths (1.78 Å, Figure 4b) are longer by ~11% than the vanadyl bond length in bulk γ-V_2O_5 (1.60 Å). In contrast, the V_B sites cannot reach any vanadyl oxygen of the layer underneath for bond formation (Figure 4c). Thus, depending on the local geometry of the V sites at the γ-V_2O_5-(001) surface, the energy to create an isolated defect differs by ~1.5 eV/atom (Table 3).

The vacancy concentration $\Theta = 1/6$ ML represents the isolated vacancy limit. Increasing the concentration to 1/4 ML changes the defect energies by <20 meV/atom because defects are still separated by four $V-O^3$ bonds (~7.2 Å) and no defect pairs at neighboring vanadyl sites are formed. For defect concentrations of 1/3 ML and higher, structures with the maximum number of V_A defects are preferred. Their averaged vacancy formation energies are shown in Figure 3. Up to 1/2 ML, the structures have defects *only* at V_A sites. Moreover, as found for α-V_2O_5, structures with V_A defects forming pairs ($\Theta = 1/3$) and rows ($\Theta = 1/2$) along the [010] direction are increasingly *easier* to form than isolated defects. Thus, for the (001) surface of both polymorphs, reduction will *not* occur by random abstraction of vanadyl oxygen atoms but rather along the [010] rows in a concerted way.[40]

The preference for the [010] alignment over other defect structures is due to cooperative relaxation effects as the vacancy concentration increases from 1/6 to 1/2 ML, that is, to sharing of

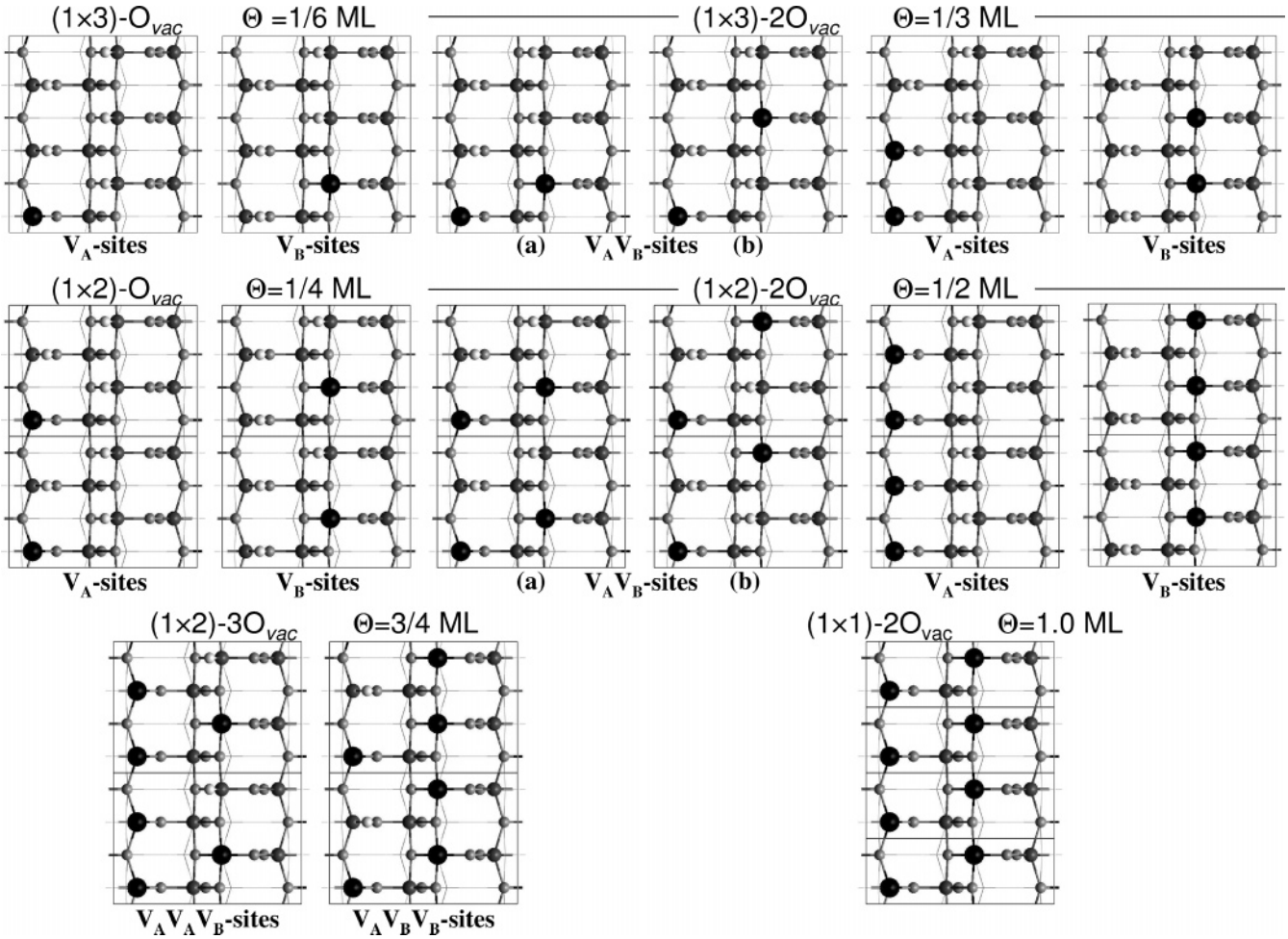

Figure 2. Schematic top view of all superstructures investigated as a function of the surface vanadyl oxygen defect concentration, Θ, in monolayers (MLs). The large black circles correspond to the surface vacancy sites and the smaller light and dark gray circles to V and O atoms at the surface layer, respectively. Vanadyl O atoms sticking *out* of the surface are depicted as small white circles. The second substrate layer is displayed using thinner sticks.

TABLE 3: Average Vanadyl Oxygen Vacancy Formation Energy, $E_f^{(1/2)O_2}$ (in eV/Atom), for the Unrelaxed and Relaxed Structures at Different Vacancy Concentrations on γ-V_2O_5(001)

Θ (ML)	structure	reduced sites	unrelaxed	relaxed
$^1/_6$	(1 × 3)-O_{vac}	V_A	3.86	1.91[a]
		V_B	3.72	3.38
$^1/_4$	(1 × 2)-O_{vac}	V_A	3.87	1.89
		V_B	3.71	3.39
$^1/_3$	(1 × 3)-2O_{vac}	V_AV_A	3.86	1.80
		V_BV_B	3.69	2.95
		V_AV_B (a)	3.82	2.68
		V_AV_B (b)	3.77	2.64
$^1/_2$	(1 × 2)-2O_{vac}	V_AV_A	3.86	1.76
		V_BV_B	3.72	3.16
		V_AV_B (a)	3.82	2.71
		V_AV_B (b)	3.83	2.63
$^3/_4$	(1 × 2)-3O_{vac}	$V_AV_AV_B$	3.86	2.32
		$V_AV_BV_B$	3.82	2.63
1.0	(1 × 1)-2O_{vac}	V_AV_B	3.88	2.53

[a] Reference 41.

the energy cost of inverting the VO_5 pyramid. Figure 4d shows the atomic geometry of the structure at $^1/_3$ ML with defects at V_A sites. The lattice relaxations resulting from an isolated defect (see Figure 4b) are not counteracted by the subsequent vacancy. The latter in turn starts forming the line defect. The (nonaveraged) energy of formation of this additional defect forming a [010]-oriented pair is by ∼0.2 eV/atom smaller than that for the isolated defect. If the subsequent defect is at a V_B site, its formation energy is by ∼1.5 eV/atom larger. In contrast to γ-V_2O_5, at the α-V_2O_5 surface, the formation of an additional defect not forming a [010]-oriented pair is only by ∼0.1 eV/atom larger due to interlayer bond formation. Thus, reducing sites *away* from the [010] trenches is significantly less likely for γ-V_2O_5(001).

Higher defect concentrations ($^3/_4$ and 1.0 ML) can only be reached if defects are also created at V_B sites and the average defect formation energy increases up to ∼0.7 eV/atom (1.0 ML) compared to the missing-row structure at $^1/_2$ ML. In contrast, at the α-V_2O_5 surface, the concentration increase results in values that are up to ∼0.2 eV/atom larger (see Figure 3).

V. Thermodynamic Stability of Reduced γ-V_2O_5(001)

We use statistical thermodynamics to take into account the effect of temperature and oxygen pressure on the stability of the reduced surfaces. The formalism has been applied to a variety of systems before (see, for example, refs 45−48). We follow here our previous work on the α-V_2O_5(001) surface[9] and consider the reduced γ-V_2O_5(001) surfaces in equilibrium with O_2 in the gas phase:

$$\gamma\text{-}V_2O_5^{\text{clean}} \rightleftharpoons \gamma\text{-}V_2O_5^{\text{vac}} + N_{\text{vac}}\frac{1}{2}O_2 \qquad (2)$$

The accompanying change of the surface free energy, $\Delta\gamma$, as a

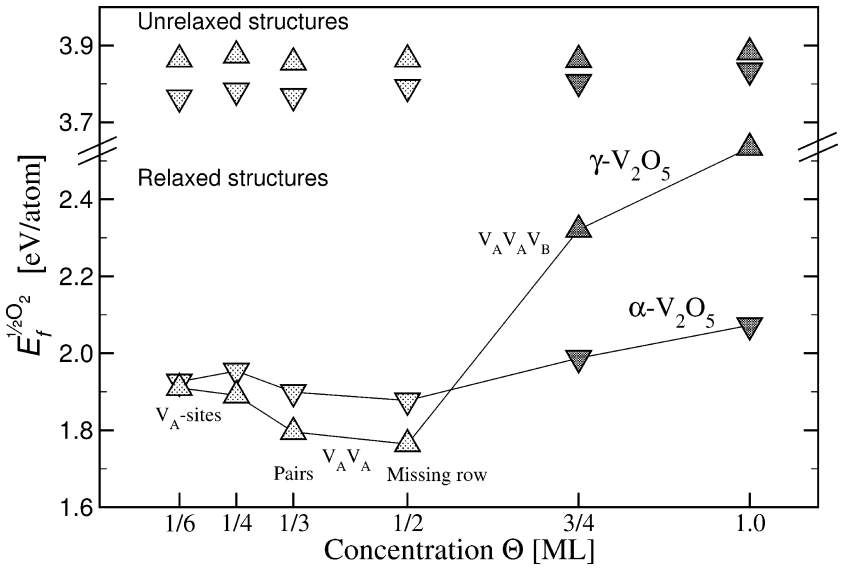

Figure 3. (lower panel) Lowest values of average vacancy formation energies in electronvolts per atom as a function of the vacancy concentration, Θ, on γ-V_2O_5(001) (up-oriented triangles). The light triangles correspond to structures in which vacancies are at V_A sites ($^1/_6$ ML ≤ Θ ≤ $^1/_2$ ML) and the darker triangles to higher defect concentrations. The down-oriented triangles show the corresponding results for α-V_2O_5(001) (ref 9). (upper panel) The values for the unrelaxed structures of the lower panel.

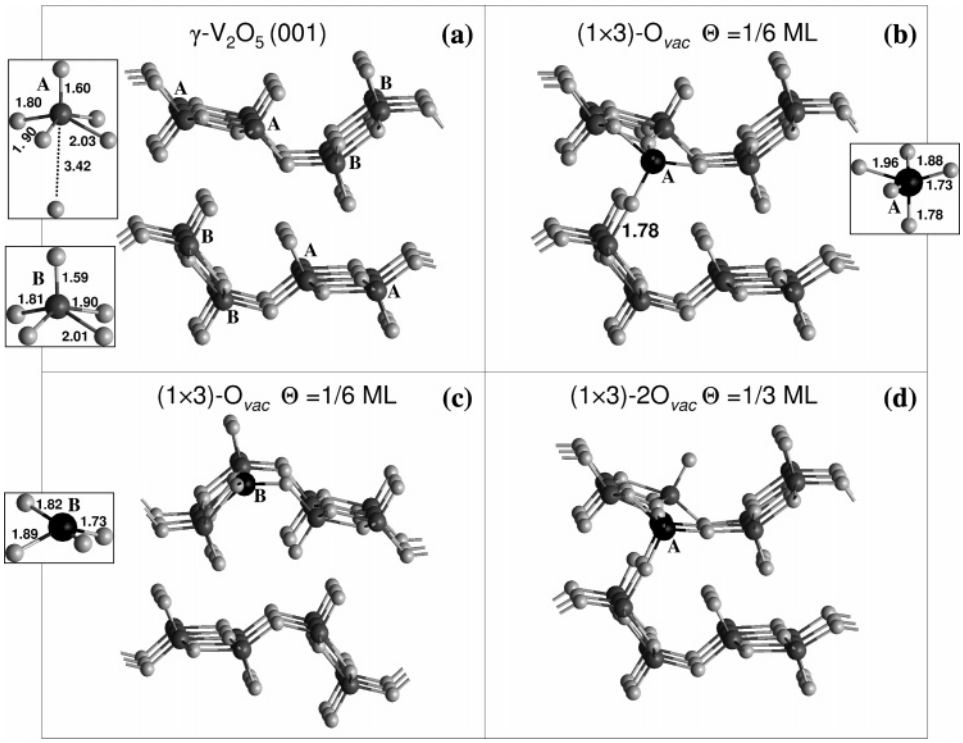

Figure 4. Atomic geometry of (a) the defect-free γ-V_2O_5(001) surface and (b) the structure at Θ = $^1/_6$ ML with a single defect at a V_A site. Part c is similar to part b, but the reduced site is of the V_B type. Part d displays the structure at Θ = $^1/_3$ ML with a pair of defects at V_A sites. The vacancy site is depicted as the large black circle, and V and O atoms are depicted as dark and light gray circles, respectively. The selected bond lengths are in angstroms.

function of the vacancy concentration, Θ, is

$$\Delta\gamma(T, p, \Theta) = \frac{1}{A}\left[E_{\mathrm{vac}}(\Theta) - E_{\mathrm{clean}} + N_{\mathrm{vac}}\frac{1}{2}\mu_{O_2}(T, p)\right] \quad (3)$$

Here, the Gibbs free energies of the solid components have been approximated by the calculated DFT total energies that are evaluated at a certain volume of the unit cell, V, and $T = 0$ K. This means that contributions which depend on the vibrational states of the systems and those resulting from the pV term are neglected. A is the area of the surface unit cell and $^1/_2\mu_{O_2}(T, p)$ the oxygen chemical potential. The difference $\Delta\gamma$ is negative if the reduced surface is more stable than the defect-free surface.

Inserting $\Delta\mu_O(T, p) = {}^1/_2[\mu_{O_2}(T, p) - E_{O_2}]$ into eq 3 and using eq 1, we obtain

$$\Delta\gamma(T, p, \Theta) = \frac{N_{\mathrm{vac}}}{A}[E_{\mathrm{f}}^{(1/2)O_2}(\Theta) + \Delta\mu_O(T, p)] \quad (4)$$

As the surrounding O_2 atmosphere forms an ideal gas reservoir, the pressure dependence of $\Delta\mu_O(T, p)$ at a given temperature is given by

$$\Delta\mu_O(T, p) = \frac{1}{2}[H(T, p^\circ) - H(0\ \mathrm{K}, p^\circ) - TS(T, p^\circ) + RT\ln(p/p^\circ)] \quad (5)$$

using $\mu_{O_2}(0\ \mathrm{K}) = E_{O_2}$. p° is the pressure of a reference state ($p^0 = 1$ atm). Tabulated values for the enthalpy, H, and entropy, S, at the temperature T were used.[49]

For a given oxygen chemical potential, we predict which surface structure is the most stable by searching for the surface model with the lowest surface free energy. Figure 5a shows the result of eq 4 for selected defect phases at the γ-V_2O_5(001) surface, namely, $^1/_6$ ML with defects at either V_A or V_B sites, the most stable phases at $\Theta = {}^1/_2$ and $^3/_4$ ML, respectively, and the fully reduced surface. For comparison, the corresponding results for the α-V_2O_5(001) surface are shown in Figure 5b (ref 50). The chemical potential, $\Delta\mu_O$, is translated into a pressure scale for a given temperature using eq 5 (see upper x-axis in Figure 5).

For the highest chemical potentials, so much oxygen is present in the gas phase that the defect-free V_2O_5(001) surfaces are most stable. Toward lower chemical potentials (lower than 1.76 eV), the $^1/_2$ ML phases with a trenchlike defect structure (defects at V_A sites for γ-V_2O_5) become more stable. Typical reducing conditions correspond, for example, to 800 K and UHV ($p < 10^{-12}$ atm). At this temperature, an oxygen chemical potential of -1.76 eV implies an oxygen partial pressure of $\sim 3 \times 10^{-12}$ atm. Thus, both the α- and γ-V_2O_5(001) surfaces should become partially reduced at 800 K UHV conditions. At 800 K and for oxygen poorer conditions, the missing-row phase remains the thermodynamically most stable structure for γ-V_2O_5(001) only. (The other (even more) reduced surfaces are all higher in energy.)

In contrast, on the α-V_2O_5 surface, the remaining vanadyl oxygen atoms are thermally *non*stable if the pressure is further reduced beyond 10^{-18} atm or the temperature is further increased under UHV conditions. Figure 5 also shows the pressure scale for $T = 1000$ K. At this temperature, the crossover between the missing-row structure and a completely reduced α-V_2O_5 surface oxygen chemical potential of -2.27 eV corresponds to $\sim 1.5 \times 10^{-12}$ (UHV). Thus, continuous reduction of the partly reduced α-V_2O_5(001) surface is possible in UHV by heating. In contrast, the remaining vanadyl atoms on the γ-V_2O_5(001) surface are stable at 1000 K and UHV. Here, it is important to mention that the PW91 functional tends to overestimate formation and binding energies which means that the calculated chemical potentials may shift by several 100 meV. Thus, the absolute pressures may change by 2−3 orders of magnitude. Nevertheless, the general stability trend is valid.

VI. Discussion

On the basis of the energies of all calculated defect structures at the (001) surfaces of both γ-V_2O_5 and α-V_2O_5, we suggest the facile reduction of both surfaces up to $\Theta = {}^1/_2$ ML due to a concerted lattice relaxation effect induced by the subsequent removal of vanadyl O atoms from V_A sites leading to [010]-oriented trenches (line defects) with (1×1) periodicity. Conversely, extending the surface reduction from $\Theta = {}^1/_2$ ML until eventually the whole surface is reduced is easier for the α-V_2O_5 surface than for the γ-V_2O_5 surface. This difference is due to the creation of defects at V_B sites at higher concentrations for the γ-V_2O_5 surface, which are not weakly bound to the layer underneath and thus less easy to reduce.

Under reducing conditions (low oxygen partial pressure and $T = 800$ K), the missing-row structure at $\Theta = {}^1/_2$ ML on both

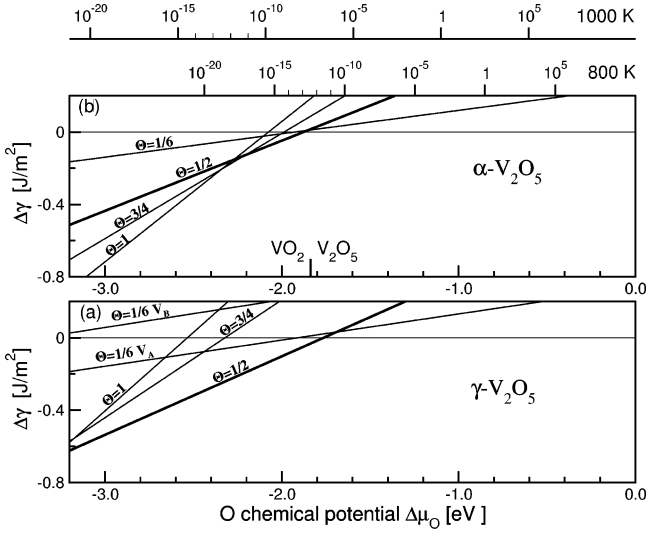

Figure 5. Surface energy change, $\Delta\gamma(T, p, \Theta)$, as a function of the chemical potential, $\Delta\mu_O$, and vacancy concentration, Θ, for the (a) γ-V_2O_5(001) and (b) α-V_2O_5(001) surfaces. In the upper x-axis, $\Delta\mu_O(T, p)$ has been translated into a pressure scale in atm at $T = 1000$ K and $T = 800$ K. The thicker lines in parts a and b correspond to the structures at $\Theta = {}^1/_2$ ML with vacancies along the [010] direction. The value of $\Delta\mu_O$ below which bulk α-V_2O_5 would be reduced to VO_2 is indicated at the lower x-axis in part b (see ref 51).

α- and γ-V_2O_5 surfaces is the thermodynamically most stable structure. At higher temperatures (1000 K) and UHV, the remaining vanadyl oxygen species are stable at the γ-V_2O_5 surfaces (V_B sites) but unstable at the α-V_2O_5 surfaces. This instability indicates again that a considerable reduction of the α-V_2O_5 surface may be easier to obtain compared to γ-V_2O_5.

We now turn briefly to the vacancy induced relaxation effect on the electronic structure of the reduced surface (see ref 9 for further details). Since neutral oxygen atoms are removed, *formally* two electrons are left at the vacancy sites. Upon relaxation (i.e., formation of a V−O−V bond with the layer underneath), these two electrons localize on the V_A defect site and the V_B site of the layer underneath. Thus, the V_A defect sites are not reduced to V^{III} but V^{IV}. Schematically,

$$\begin{array}{ccccc} \mathrm{O} & & & & \\ \| & & & & \\ \mathrm{V_A^{V}} & & \mathrm{V_A^{III}} & & \mathrm{V_A^{IV}} \\ \vdots & \xrightarrow{-\mathrm{O}} & \vdots & \xrightarrow{\mathrm{relax}} & | \\ \mathrm{O} & & \mathrm{O} & & \mathrm{O} \\ \| & & \| & & | \\ \mathrm{V_B^{V}} & & \mathrm{V_B^{V}} & & \mathrm{V_B^{IV}} \end{array}$$

In contrast, the reduction of V_B sites yields V^{III} centers. The highest spin state was found to be most stable for all the γ-V_2O_5 reduced surfaces considered. We note that the PW91 functional tends to delocalize the electrons somewhat beyond the defect site and its counterpart at the second layer.[42]

A previous DFT study has shown that the reduction of surface vanadyls terminating thin vanadium oxide films supported on α-Al_2O_3(0001) is less facile than the reduction of surface vanadyls on crystalline V_2O_5(001) (ref 43). Reduction yields V^{III} centers, and the vanadyl binding energy is comparable to the value for an isolated defect at a V_B site at the γ-V_2O_5(001) surface. Such a behavior was also attributed to the fact that the presence of the alumina support does not allow for significant

lattice relaxations upon defect formation. The correlation between local structure and reducibility is further substantiated by experimental studies on thick $V_2O_3(0001)$ films on Au(111) and W(110) for which terminating vanadyl oxygen atoms are stable until at least 1000 K in UHV (ref 44). The results obtained in this work suggest that γ-V_2O_5 may be used as a model system to study selective oxidation, since, similar to the supported oxides, the reducibility of this phase is lower than that of the α-V_2O_5 phase. The presence of V_B sites modifies the surface reducibility and in turn may lead to a modified catalytic behavior.

Acknowledgment. This work has been supported by the Deutsche Forschungsgemeinschaft (SFB 546) and the Fonds der chemischen Industrie. We are grateful to R. Schlögl, M. Willinger, and A. Hofmann for useful discussions. The calculations were carried out at the IBM p690 system of the Nordeutscher Verbund für Hoch- und Höchstleistungsrechnen (HLRN). We thank B. Kallies for technical support.

References and Notes

(1) Bañares, M. A. *Catal. Today* **1999**, *51*, 319.
(2) Weckhuysen, B. M.; Keller, D. E. *Catal. Today* **2003**, *78*, 25.
(3) Mars, P.; van Krevelen, D. W. *Spec. Suppl. Chem. Eng. Sci.* **1954**, *3*, 41.
(4) Chen, K.; Khodakov, A.; Yang, J.; Bell, A. T.; Iglesia, E. *J. Catal.* **1999**, *186*, 325.
(5) Chen, K.; Iglesia, E.; Bell, A. T. *J. Catal.* **2000**, *192*, 197.
(6) Chen, K.; Bell, A. T.; Iglesia, E. *J. Phys. Chem. B* **2000**, *104*, 1292.
(7) Argyle, M. D.; Chen, K.; Resini, C.; Krebs, C.; Bell, A. T.; Iglesia, E. *Chem. Commun.* **2003**, 2082.
(8) Argyle, M. D.; Chen, K.; Resini, C.; Krebs, C.; Bell, A. T.; Iglesia, E. *J. Phys. Chem. B* **2004**, *108*, 2345.
(9) Ganduglia-Pirovano, M. V.; Sauer, J. *Phys. Rev. B* **2004**, *70*, 045422.
(10) Cocciantelli, J. M.; Gravereau, P.; Doumerc, J. P.; Pouchard, M.; Hagenmuller, P. *J. Solid State Chem.* **1991**, *93*, 497.
(11) Willinger, M.; Pinna, N.; Su, D. S.; Schlögl, R. *Phys. Rev. B* **2004**, *69*, 155114.
(12) Pinna, N.; Wild, U.; Urban, J.; Schlögl, R. *Adv. Mater.* **2003**, *15*, 329.
(13) Pinna, N.; Willinger, M.; Weiss, K.; Urban, J.; Schlögl, R. *Nano Lett.* **2003**, *3*, 1131.
(14) Hohenberg P.; Kohn, W. *Phys. Rev.* **1964**, *136*, 864.
(15) Kohn, W.; Sham, L. J. *Phys. Rev.* **1965**, *140*, 1133.
(16) Kresse, G.; Hafner, J. *Phys. Rev. B* **1993**, *48*, 13115.
(17) Kresse, G.; Furthmüller, J. *Comput. Mater. Sci.* **1996**, *6*, 15.
(18) Kresse, G.; Furthmüller, J. *Phys. Rev. B* **1996**, *54*, 11169.
(19) The version VASP.4.6.12 released on June 27, 2003 has been used.
(20) Perdew, J. P.; Chevary, J. A.; Vosko, S. H.; Jackson, K. A.; Pederson. M. R.i; Singh, D. J.; Fiolhais, C. *Phys. Rev. B* **1992**, *46*, 6671; **1992**, *48*, 4978.
(21) Blöchl, P. E. *Phys. Rev. B* **1994**, *50*, 17953.
(22) Monkhorst, H. J.; Pack, J. D. *Phys. Rev. B* **1976**, *13*, 5188.
(23) The calculated total energies for the O atom and O_2 molecule are $-1.770\,40$ and $-9.794\,44$ eV, respectively.
(24) Herzberg, G. *Molecular Spectra and Molecular Structure. I. Spectra of Diatomic Molecules*, 2nd ed.; Robert E. Krieger Publishing Co., Inc.: Malabar, FL, 1989.
(25) Perdew, J. P.; Burke, K.; Ernzerhof, M. *Phys. Rev. Lett.* **1996**, *77*, 3865; **1997**, *78*, 1396.
(26) Zhang, Y.; Yang, W. *Phys. Rev. Lett.* **1998**, *80*, 890.
(27) Murnaghan, F. D. *Proc. Natl. Acad. Sci. U.S.A.* **1944**, *30*, 244.
(28) Enjalbert, R.; Galy, J. *Acta Crystallogr., Sect. C* **1986**, *42*, 1467.
(29) The calculated total energies for bulk α-V_2O_5, γ-V_2O_5, and bcc vanadium are $-58.759\,28$, $-58.701\,55$, and $-8.930\,00$ eV/formula unit, respectively.
(30) Linstron, P. J., Mallard, W. G., Eds. *NIST Chemistry WebBook*; National Institute of Standards and Technology: Gaithersburg, MD, 2001 (http://webbook.nist.gov).
(31) Ruberto, C.; Yourdshahyan, Y.; Lundqvist, B. I. *Phys. Rev. B* **2003**, *67*, 195412.
(32) Wolwerton, C.; Haas, K. C. *Phys. Rev. B* **2001**, *63*, 024102.
(33) Yokokawa, T.; Kleppa, O. J. *J. Phys. Chem.* **1965**, *68*, 3246.
(34) Tsuzuki, S.; Jacobsen, K. W.; Nørskov, J. K. *J. Chem. Phys.* **2001**, *114*, 3949.
(35) Rydberg, H.; Dion, M.; Jacobson, N.; Schröder, E.; Hyldgaard, P.; Simak, S. I.; Langreth, D. C.; Lundqvist, B. I. *Phys. Rev. Lett.* **2003**, *91*, 126402.
(36) Bollinger, M. V.; Jacobsen, K. W.; Nørskov, J. K. *Phys. Rev. B* **2003**, *67*, 085410.
(37) Rydberg, H.; Jacobson, N.; Hyldgaard, P.; Simak, S. I.; Lundqvist, B. I.; Langreth, D. C. *Surf. Sci.* **2003**, *532*, 606.
(38) Fiermans, L.; Vennik, J. *Surf. Sci.* **1968**, *9*, 187.
(39) Theis, W. (Free University Berlin), personal communication, 2004.
(40) For α-$V_2O_5(001)$, $E_f^{(1/2)O_2} = 1.93$, 1.90, and 1.87 eV/atom at $\Theta = {}^1/_6$, ${}^1/_3$, and ${}^1/_2$, respectively. For the missing-row structure at $\Theta = {}^1/_2$ ML on α-$V_2O_5(001)$, the calculated total energies are $E_{vac}(\Theta) = -456.117\,35$ eV and $E_{clean} = -469.666\,28$ eV.
(41) For the missing-row structure at $\Theta = {}^1/_2$ ML on γ-$V_2O_5(001)$, the calculated total energies are $E_{vac}(\Theta) = -456.064\,74$ eV and $E_{clean} = -469.386\,47$ eV.
(42) Sauer, J.; Döbler, J. *J. Chem. Soc., Dalton Trans.* **2004**, *19*, 3116.
(43) Brázdová, V.; Ganduglia-Pirovano, M. V.; Sauer, J. *Phys. Rev. B* **2004**, *69*, 165420.
(44) Dupuis, A.-C.; Abu Haija, M.; Richter, B.; Kuhlenbeck, H.; Freund H.-J. *Surf. Sci.* **2003**, *539*, 99.
(45) Scheffler, M. *Physics of Solid Surfaces-1987*; Koukal, J., Ed.; Elsevier: Amsterdam, The Netherlands, 1988. Scheffler, M.; Dabrowski, J. *Philos. Mag. A* **1988**, *58*, 107.
(46) Kaxiras, E.; Bar-Yam, Y.; Joannopoulos, J. D. *Phys. Rev. B* **1987**, *35*, 9625.
(47) Qian, G.-X.; Martin, R. M.; Chadi, D. J. *Phys. Rev. B* **1988**, *38*, 7649.
(48) Zhang, S. B.; Northrup, J. E. *Phys. Rev. Lett.* **1991**, *67*, 2339.
(49) Stull, D. R., Prophet, H., Eds.; *JANAF Thermochemical Tables*, 2nd ed.; U.S. National Bureau of Standards: Washington, DC, 1971.
(50) In ref 9, $\Delta\gamma/2$ is shown in Figure 10.
(51) The condition for $\Delta\mu_O$ for which the lower VO_2 bulk oxide is thermodynamically more stable than the α-V_2O_5 is $\Delta\mu_O < E_f^{\alpha-V_2O_5} - 2E_f^{VO_2}$. We obtain $\Delta\mu_O = -1.84$ eV for this bound. Since this value is not significantly different from the value -1.87 eV below which the missing-row structure at the α-$V_2O_5(001)$ surface becomes more stable, we suggested that the reduction that starts at the surface may initiate the conversion to the lower bulk oxide (see ref 9).